Tube Dynamics Works for Randomly Entangled Rings

Jian Qin and Scott T. Milner

Phys. Rev. Lett. **116**, 068307 — Published 12 February 2016

DOI: 10.1103/PhysRevLett.116.068307

Tube dynamics works for randomly entangled rings

Jian Qin*[1] and Scott T. Milner[2]

[1]*Department of Chemical Engineering, Stanford University, Stanford, CA 94305, USA*
[2]*Department of Chemical Engineering, Pennsylvania State University, State College, PA 16802, USA*

(Dated: January 25, 2016)

The tube model is the cornerstone of molecular theory for polymer rheology. We test its microscopic assumptions by simulating topologically equilibrated ring polymers, whose dynamics is free from end segment relaxation. We show that a closed-form expression derived from the tube model adapted to ring polymers quantitatively predicts the segmental mean squared displacements over the entire range of timescales from local motion to complete equilibration, with a time-independent local friction factor.

Stress relaxation in polymer liquids is inconveniently slow because of molecular entanglement [1]: the chain–like molecules interweave with their neighbors, and mutually restrict sideway motions because they cannot pass through each other. This phenomenon is generally accounted for by using the tube theory [2, 3], which asserts that polymers move as if they are confined inside a tube–like region. They are free to wiggle and creep along the tube contour, but their transverse motions are constrained. The strength of confinement is quantified by the tube diameter a, which is treated as a material parameter to be determined by comparing measured rheological responses with tube theory predictions [4].

The modern theory of polymer rheology was developed by incorporating various tube relaxation mechanisms [5, 6]. The predominant mechanism is reptation, which is the curvilinear diffusion of polymers along the tube contour [3]. Incorporating reptation and two other mechanisms, constraint release (CR) [3, 7–9] and contour length fluctuation (CLF) [10–12], into a coherent framework has yielded a highly successful molecular theory for polymer rheology, tested in both the linear [13] and nonlinear [14, 15] regimes.

Despite its marvelous success in capturing the macroscopic phenomenology, the microscopic assumptions of the tube model have not been thoroughly scrutinized. An early molecular dynamics (MD) simulation [16] revealed the tube by visualizing chain motions. Later, more detailed analyses focused on the bead mean squared displacement (MSD), an elementary dynamical quantity [16–18]. According to the tube model, for sufficiently long chains the bead MSD exhibits three dynamical regimes preceding free diffusion, with time-scaling exponents 1/2, 1/4 and 1/2 respectively [1].

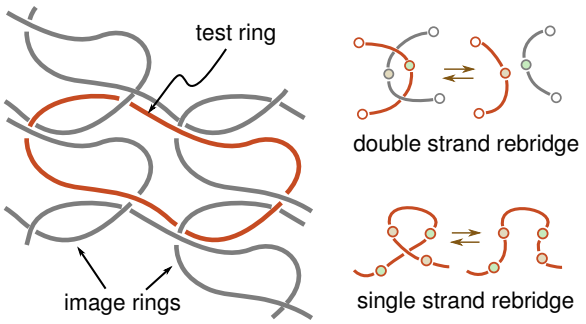

FIG. 1: Left: a ring polymer entangled with its periodic images. Right: ring rebridging moves, which equilibrate the entanglement topology.

The first two regimes were verified by simulations [16–18] and by neutron spin–echo experiments [19]. The third regime, with slope 1/2, has never been unambiguously observed. A recent work at best identified a 1/4-to-diffusion crossover [18]. The lack of a distinct third regime results from the finite length of the chains, which compresses the width of the regime, and introduces corrections from chain end motions, an unavoidable complication for linear chains.

Doubts about the tube theory have never been scarce. Motivated by recent experiments [20] and simulations [21, 22], fundamental assumptions of the theory have been questioned [23] and defended [24, 25]. More cautious refinements were also suggested, e.g., that the bead friction factor, a key parameter in the model, may depend on the range and time scale of motion [26, 27].

Are we indeed at a "turning point" [23], with the tube model in jeopardy? To provide a new quantitative test of the tube theory, we study the dynamics of long, randomly entangled ring polymers. We shall show that the dynamics of randomly entangled rings is an excellent proxy for entangled linear chains, with the useful simplification that the complicating effects of chain ends are absent. Indeed, our simulations of bead MSD for rings clearly display the tube model scaling regimes, except for self-diffusion at long times (since the rings are permanently linked). Our analyses show that the entire MSD versus time, including crossovers, can be quantitatively captured by the tube theory adapted to ring polymers, an agreement not previously achieved for linear chains.

We emphasize that to test the tube model, studying *randomly linked* rings is essential. Several recent works [28–31] have investigated the dynamics of melts of *unlinked* rings, and found an unusual $t^{-1/2}$ stress relaxation rate [31], very different from entangled linear chains.

The system of concatenated ring polymers we studied

is schematically shown in Fig. 1. In addition to eliminating chain end effects, ring polymers afford another advantage: all chain segments are statistically equivalent, so the quality of MSD data can be improved by averaging over all beads. However, the absence of free ends also makes it impossible to equilibrate the topology by MD simulation alone. We must introduce Monte Carlo (MC) moves designed to alter local chain connectivity, thus allowing rings to cross [32].

We use a standard bead–spring model for polymers [32]. All non-bonded beads interact via the WCA potential [33], which is a purely repulsive, truncated and shifted Lennard-Jones potential. The bond energy is harmonic, of form $\kappa(r_{ij}-\sigma)^2/2$, where r_{ij} is the separation between bonded beads and σ the bond rest length. A large spring constant $\kappa = 400\, k_{\rm B}T\sigma^{-2}$ keeps bonded beads close together, so chains cannot pass through each other.

Our system consists of a single long ring of N beads, in a cubic box with periodic boundary conditions (PBC). The box dimension is chosen so that the bead number density is $\rho = 0.7\,\sigma^{-3}$, which is dense enough to represent a melt [34, 35]. The initial ring configuration is generated by first building a random walk of $N-1$ steps, then distributing the end–to–end distance vector to all N bonds to close the walk, and folding the ring into the simulation box by applying the PBC. To explore the effects of ring length, we studied three systems with $N = 400$, 800, and 1600. For each N, we prepared 10 independent replicas, to average over the entanglement configuration. All MSD data reported below are averages over all beads in the system and over all 10 replicas.

The ring configurations are equilibrated using MC moves. We first apply bead random displacement moves to eliminate unphysical overlaps. Then we relax the pressure with hybrid MC/MD moves, in which the configuration is propagated by a short MD integration, and the new configuration accepted according to the Metropolis rule. Next, we equilibrate the entanglement topology, by turning on a family of rebridging MC moves (for details, see Ref. [32]).

Two simple rebridging moves are shown in Fig. 1. The acceptance rates are 96% for hybrid MC/MD moves, 0.45% for single strand single rebridging moves, 0.036% for single strand double rebridging moves, and 0.027% for double strand rebridging moves (not shown). The number of equilibration MC steps is typically 6×10^9. Conformational equilibrium is verified by making sure that ring Rouse modes decorrelate in time [32], and that our rings display random walk statistics, as expected for a dense melts of topologically equilibrated rings.

After topological equilibration, we turn off the rebridging moves, and use NVT ensemble MD simulation to collect data on bead MSD. The MD integration step unit is $0.005\,\tau$, where τ equals $\sigma(m/\epsilon)^{1/2}$, σ and ϵ are the interaction range and strength of WCA potential, and m is the bead mass. The Nosé-Hoover thermostat is used and the temperature is held at $k_{\rm B}T = \epsilon$. With rebridging moves turned off, we are observing the dynamics of ring polymers inside a tube with fixed topology. We average over the specific tube topology by averaging the bead MSD over the 10 replicas. To efficiently analyze the MSD data spanning a long time range, a multi-τ correlator [36] is implemented. The final results for all three ring lengths are presented in Fig. 2, with the errorbars representing the standard deviation over 10 replicas.

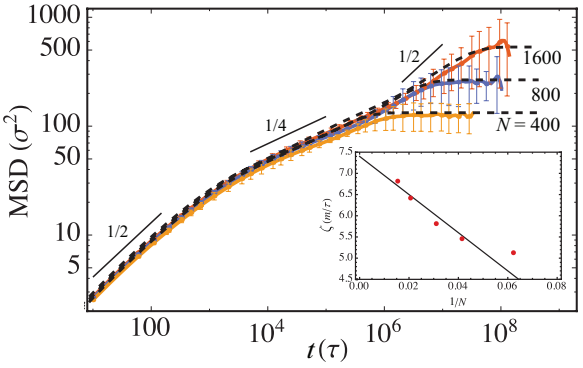

FIG. 2: Bead mean squared displacements, for three rings with $N = 400$, 800 and 1600; MD results (solid) and tube theory predictions (dashed). Inset: friction factors ζ from linear chain simulations, with fit of form $\zeta(N) = \zeta(\infty) - c/N$.

The data display two prominent features. First, for time less than $10^5\,\tau$, the N-dependence is very weak. All three data sets exhibit the first two tube model scaling regimes, with predicted exponents 1/2 and 1/4 [1]. Second, for much later time, all data sets reach an N-dependent plateau, beyond which bead MSD is constant. This plateau is expected for randomly entangled ring polymers, for which entanglements are permanent and ring self-diffusion is suppressed. The later $t^{1/2}$ scaling regime [1] expected between the $t^{1/4}$ and plateau regimes, is slightly visible only for the $N = 1600$ case. All these trends, as well as crossovers between regimes, can be predicted by the tube theory adapted to ring polymers, presented below. The predictions are shown as dashed lines in Fig. 2.

Our theory treats the short and long time dynamics separately. At short times, in regime I of Fig. 3, the beads do not feel the tube confinement, and the chain moves by 3D Rouse motion [1]. At later times, in regimes II, III and IV, the beads explore the tube by 1D Rouse motion, and their MSD conforms to the region of tube contour explored. As illustrated in Fig. 3, the tube contour may be described by a random ring with step size of the tube diameter a. The number of steps is $Z \equiv N/N_{\rm e}$ and the contour length is $L = Za$, where $N_{\rm e} \equiv (a/b)^2$ is the entanglement molecular weight [1].

The treatment of dynamics in regime I is identical to

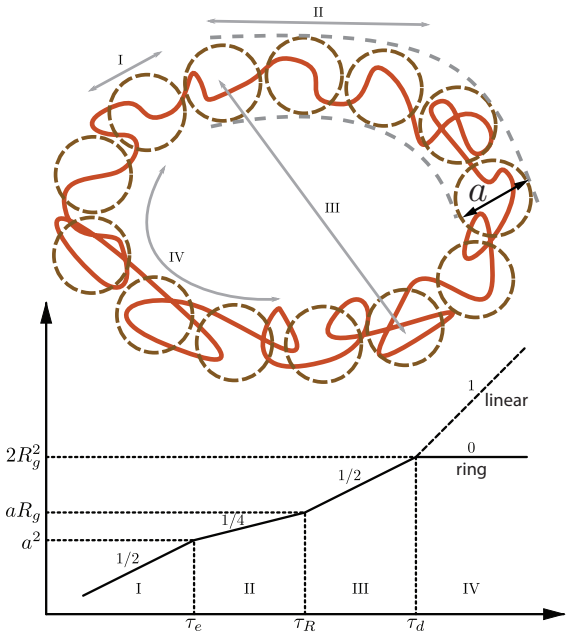

FIG. 3: Expected regimes of bead MSD regimes for tube model. I: beads do not feel the tube, and move by 3D Rouse dynamics. II: beads move by 1D Rouse dynamics along the tube. III: beads move by ring reptation. IV: beads have traversed the tube many times; MSD reaches a plateau.

that for linear chains. The position vector $\mathbf{R}_n$ of the nth bead obeys the Langevin equation

$$\zeta \frac{\partial \mathbf{R}_n(t)}{\partial t} = K \frac{\partial^2 \mathbf{R}_n(t)}{\partial n^2} + \mathbf{f}_n(t), \tag{1}$$

with a friction factor ζ. Chain connectivity is represented by the first term to the right, with $K = 3k_BT/b^2$ the effective spring constant for Gaussian coils [1]. The noise terms on each bead $\mathbf{f}_n(t)$ are independent and delta-correlated, with zero mean and variance given by $\langle f_{n\alpha}(t) f_{m\beta}(t')\rangle = 2\zeta k_B T \delta_{\alpha\beta}\delta_{mn}\delta(t-t')$, where α and β are coordinate indices.

Eq. (1) can be solved by introducing Rouse modes $\mathbf{X}_p(t) \equiv \frac{1}{N}\sum_{n=1}^{N} \mathrm{e}^{-\mathrm{i}2\pi pn}\mathbf{R}_n(t)$ [1]. The phase factor 2π differs from that for linear chains because of the periodic boundary condition applicable to bead indices. The mode amplitudes $\mathbf{X}_p(t)$ can be explicitly solved for any initial $\mathbf{X}_p(0)$. The bead positions $\mathbf{R}_n(t)$ and MSD $\langle \Delta\mathbf{R}_n(t)^2\rangle \equiv \langle (\mathbf{R}_n(t) - \mathbf{R}_n(0))^2\rangle$ follow from the inverse Fourier transform of $\mathbf{X}_p(t)$. Averaging $\langle \Delta\mathbf{R}_n(t)^2\rangle$ with respect to index n gives

$$\langle \Delta\mathbf{R}^2\rangle = 12\sum_{p=1}^{N/2} \frac{k_BT}{K_p}\left(1 - \mathrm{e}^{-t/\tau_p}\right), \tag{2}$$

where K_p is defined by $4\pi^2p^2K/N$. In Eq. (2) we have combined the contributions from conjugate modes with indices p and $N-p$, and omitted the self-diffusion term $p = 0$. To arrive at the final results, we have used the thermalized initial amplitudes $\langle X_{p,\alpha}(0)^2\rangle = k_BT/K_p$. Contributions from all the modes damp exponentially, with time constants $\tau_p = \zeta_p/K_p = N^2\zeta/(4\pi^2p^2K)$ that are smaller than linear chains by a factor of 4.

Changing summation in Eq. (2) to an integral, we can show that bead MSD in regime I grows as $t^{1/2}$. Alternatively, we can argue that when one bead diffuses a distance $\langle \Delta\mathbf{R}^2\rangle^{1/2}$, it is accompanied by the displacement of $\langle \Delta\mathbf{R}^2\rangle/b^2$ neighboring beads, giving rise to a time–dependent diffusion constant $D_{\mathrm{eff}} \simeq \frac{k_BT}{(\langle \Delta\mathbf{R}^2\rangle/b^2)\zeta}$. Equating $\langle \Delta\mathbf{R}^2\rangle$ with $D_{\mathrm{eff}}\,t$ leads to the same $t^{1/2}$ scaling. This scaling persists until time τ_e, at which the MSD reaches the tube diameter, when we have $\langle \Delta\mathbf{R}^2\rangle \simeq a^2 = N_e b^2$ and $\tau_e = N_e^2\zeta/(\pi^2K)$.

After τ_e, the tube confinement is effective. Beads are then displaced along the tube contour by curvilinear Rouse motion. We denote the bead displacement along tube contour by z, and nondimensionalize it by defining $s \equiv zN_e/a$. As a bead translates in s along the tube contour, it moves in space as well. Because the tube contour is a random walk, the bead MSD in space is related to the variance in s for $\delta s \gg N_e$ by $\langle \Delta\mathbf{R}^2\rangle = \langle \delta s^2\rangle^{1/2} a^2/N_e$.

At scaling level, three characteristic behaviors can be identified for MSD (Fig. 3). In regime II, bead motion is dominated by contour length fluctuations along the tube contour. The spreading $\langle \delta s^2\rangle$ scales with $t^{1/2}$ according to the Rouse model, so MSD scales with $t^{1/4}$. In regime III, the curvilinear Rouse modes have relaxed, and bead motion is dominated by reptation. The spreading $\langle \delta s^2\rangle$ increases linearly with time, so MSD scales with $t^{1/2}$. The onset time of this regime is the longest Rouse time $\tau_R \equiv \tau_1$. In regime IV, all beads have thoroughly explored the circular tube, so the MSD saturates. This happens for times beyond the diffusion time $\tau_d \equiv L^2/(N\zeta)^{-1} \propto N^3$ needed for beads to traverse the tube.

Remarkably, a closed-form expression for bead MSD can be derived, by combining the Rouse model result for the curvilinear spreading $\langle \delta s(t)^2\rangle$, with the random walk statistics of the tube itself. From the Rouse solution to the 1D version of Eq. (1), we obtain

$$\langle \delta s(t)^2\rangle = \frac{4N_e}{b^2}\sum_{p=1}^{N/2}\frac{k_BT}{K_p}\left(1 - \mathrm{e}^{-t/\tau_p}\right) + \frac{2N_e k_BT}{b^2 N\zeta}t. \tag{3}$$

Here the linear term is the reptation contribution.

To relate Eq. (3) to the real space displacement $\mathbf{R}_s$ and calculate the thermal average, we expand $\mathbf{R}_s$ in Rouse modes as $\mathbf{R}_s = {\sum_{p=-Z/2}}' \mathbf{Y}_p \mathrm{e}^{\mathrm{i}2\pi p\delta s/N}$. The bead MSD is then given by

$$\langle \Delta\mathbf{R}_s^2\rangle = 12\sum_{p=1}^{Z/2}\frac{k_BT}{K_p}\left(1 - \langle\cos\left(2\pi p\delta s(t)/N\right)\rangle\right). \tag{4}$$

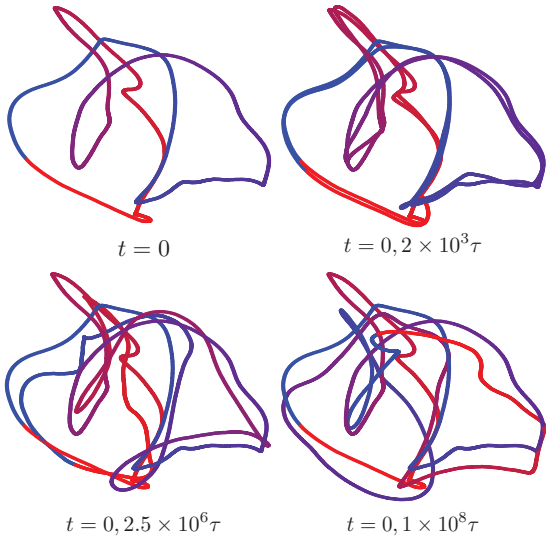

FIG. 4: Tube contours (colored red to blue by bead index) from isoconfigurational average over time $\tau_a = 2 \times 10^4\,\tau$. Different contours correspond to elapsed times τ_e, τ_R and τ_d.

The average $\langle \cos(2\pi p \delta s(t)/N) \rangle$ is evaluated by noting that $\delta s(t)$ is a Gaussian random variable with zero mean and variance given by Eq. (3). This leads to $\langle \cos(2\pi p \delta s/N) \rangle = \exp(-2\pi^2 \langle \delta s(t)^2 \rangle p^2/N^2)$. The MSD grows with time, to a maximum value at long times $12 \sum_{p=1}^{Z/2} \frac{k_B T}{K_p}$. Setting $Z = \infty$ gives the asymptotic limit $Nb^2/6 = 2R_g^2$, an expected result since, at infinite time delay, the bead MSD can be equivalently written as $N^{-2} \sum_{m,n=1}^{N} \langle (\mathbf{R}_n - \mathbf{R}_m)^2 \rangle = 2R_g^2$.

The above results can be merged with the unconstrained motion at early times $t < \tau_e$ described by Eq. (2), by assuming that modes with $1 \le p \le Z/2$ and $Z/2 < p \le N/2$ evolve by 1d curvilinear Rouse and 3D Rouse dynamics respectively (a smoother crossover function may be used in practice to improve the fitting quality). Thus we write

$$\frac{\langle \Delta \mathbf{R}^2 \rangle}{R_g^2} = \frac{12}{\pi^2} \sum_{p=\lfloor Z/2 \rfloor + 1}^{N/2} \frac{1 - e^{-4p^2 (t/\tau_e)/Z^2}}{p^2} + \frac{12}{\pi^2} \sum_{p=1}^{p=\lfloor Z/2 \rfloor} \frac{1 - e^{-2\pi^2 p^2 \langle \delta s(t)^2 \rangle / N^2}}{p^2}. \quad (5)$$

This closed–form expression contains only two parameters, the entanglement length N_e and relaxation time τ_e, which can be determined by comparison to simulation results. Note that unlike linear chains, for rings all beads are statistically equivalent, so we measure and compute the MSD averaged over all beads.

The theoretical curves in Fig. 2 are computed using Eq. (5), with parameter values $N_e = 73$ and $\tau_e = 2800\,\tau$ optimized visually. This value of N_e is consistent with our results based on purely *topological* analysis [32, 37]. The value of τ_e implies a friction factor $\zeta = 7.9\,(m/\tau)$, calculated from $\zeta = 3\pi^2 k_B T \tau_e/(N_e^2 b^2)$ [1]. We separately determined molecular diffusivity D in melts of linear chains for chain lengths $N = 16$, 24, 32, 48 and 64, and obtained the friction factors $\zeta(N) \equiv k_B T/(ND)$. By plotting against $1/N$ and extrapolating to $N = \infty$ (inset of Fig. 2), we obtain $\zeta(\infty) = 7.4\,(m/\tau)$, reassuringly close to our value from MSD for rings.

From the MSD data for $N = 1600$, we can read off Rouse and reptation times $\tau_R \sim 10^6\,\tau$ and $\tau_d \sim 10^8\,\tau$. These values are compatible with the time evolution of tube contour, visualized using ICE (isoconfigurational ensemble) average [38]. For ICE, we average over 100 short MD trajectories, all starting from the same initial configuration, but with different initial thermal velocities. Fig. 4 show ICE tube contours for $N = 1600$, colored by bead index, for different time delays from a given starting configuration. At $t = \tau_e$, the tube has barely moved; at $t = \tau_R$, the contour has wiggled a bit; by $t = \tau_d$, the contour still mostly retraces its old path, but has reptated far along its own length — as expected from the tube model and the regimes of Fig. 3. The τ_d values for $N = 800$ and 400 are close to $10^7\,\tau$ and $10^6\,\tau$, in agreement with the expected N^3 scaling.

In summary, the bead mean-square displacement for randomly entangled ring polymers can be quantitatively described by the tube model, with only the entanglement molecular weight N_e and bead friction factor ζ as fitting parameters. Our closed-form expression describes the MSD over eight orders of magnitude in time and two orders in length, for rings of 5, 10 and 20 entanglement strands, with the same values $N_e = 73$ and $\zeta = 7.9\,(m/\tau)$. These values are consistent with our topological analysis of entanglement states [32, 37] and analysis of molecular diffusivity in linear polymer melts.

The tube model fits the data well under the naive assumption that the same friction factor applies to reptation, curvilinear Rouse motion and local Rouse motion. In response to the suggested possibility of using different values in different regimes [26, 27], we suggest the opposite. The close quantitative agreement with MSD data does not resolve the controversy noted in recent simulations of strong chain stretching during startup shear [22, 24, 39], but does lend strong support to the tube theory (see also [40]).

The closed–form expression for bead MSD, Eq. (5), suggests an approach to determine N_e and ζ for real polymers, from fitting to atomistic simulations. To obtain N_e and ζ, the simulation only needs to extend well beyond τ_e, so that the first crossover from 1/2 to 1/4 can be observed, i.e., so the chain can "feel" the tube. Our expression for rings describes this crossover well. Given the modest system size and computation costs required, it should be possible to apply our methods to atomistic MD simulations of topologically equilibrated rings. Multiple systems with values of Z ranging from 5 to 10 may

suffice for such a purpose.

We acknowledge funding from NSF DMR-039744.

[1] M. Doi and S. F. Edwards, *The Theory of Polymer Dynamics* (Clarendon Press, Oxford, 1986).
[2] S. F. Edwards, Proc. Phys. Soc. **92**, 9 (1967).
[3] P. G. de Gennes, J. Chem. Phys. **55**, 572 (1971).
[4] R. G. Larson, T. Sridhar, L. G. Leal, G. H. McKinley, A. E. Likhtman, and T. C. B. McLeish, J. Rheol. **47**, 809 (2003).
[5] T. C. B. McLeish, Adv. Phys. **51**, 1379 (2002).
[6] W. W. Graessley, *Polymeric Liquids & Networks: Dynamics and Rheology* (Garland Science, New York, 2008).
[7] R. H. Colby and M. Rubinstein, J. Chem. Phys. **89**, 5291 (1988).
[8] J. L. Viovy, R. H. Colby, and M. Rubinstein, Macromolecules **24**, 3587 (1991).
[9] S. T. Milner, J. Rheol. **40**, 303 (1996).
[10] M. Doi, J. Polym. Sci. Polym. Lett. Ed. **19**, 265 (1981).
[11] M. Doi, J. Polym. Sci. Polym. Phys. Ed. **21**, 667 (1983).
[12] S. T. Milner and T. C. B. McLeish, Phys. Rev. Lett. **81**, 725 (1998).
[13] A. E. Likhtman and T. C. B. McLeish, Macromolecules **35**, 6332 (2002).
[14] S. T. Milner, T. C. B. McLeish, and A. E. Likhtman, J. Rheol. **45**, 539 (2001).
[15] R. S. Graham, A. E. Likhtman, T. C. B. McLeish, and S. T. Milner, J. Rheol. **47**, 1171 (2003).
[16] K. Kremer and G. S. Grest, J. Chem. Phys. **92**, 5057 (1990).
[17] M. Pütz, K. Kremer, and G. S. Grest, Europhys. Lett. **49**, 735 (2000).
[18] Z. Wang, A. E. Likhtman, and R. G. Larson, Macromolecules **45**, 3557 (2012).
[19] A. Wischnewski, M. Monkenbusch, L. Willner, D. Richter, and G. Kali, Phys. Rev. Lett. **90**, 058302 (2003).
[20] S.-Q. Wang, Y. Wang, S. Cheng, X. Li, X. Zhu, and H. Sun, Macromolecules **46**, 3147 (2013).
[21] Y. Lu, L. An, S.-Q. Wang, and Z.-G. Wang, Macromolecules **47**, 5432 (2014).
[22] Y. Lu, L. An, S.-Q. Wang, and Z.-G. Wang, Macromolecules **48**, 4164 (2015).
[23] S.-Q. Wang, Soft Matter **11**, 1454 (2015).
[24] Y. Masubuchi and H. Watanabe, ACS Macro Lett. **3**, 1183 (2014).
[25] R. S. Graham, E. P. Henry, and P. D. Olmsted, Macromolecules **46**, 9849 (2014).
[26] A. E. Likhtman, S. K. Sukumaran, and J. Ramírez, Macromolecules **40**, 6748 (2007).
[27] A. E. Likhtman, J. Non-Newtonian Fluid Mech. **157**, 158 (2009).
[28] T. Vettorel, S. Y. Reigh, D. Y. Yoon, and K. Kremer, Macromol. Rapid Commun. **30**, 345 (2009).
[29] J. D. Halverson, W. B. Lee, G. S. Grest, A. Y. Grosberg, and K. Kremer, J. Chem. Phys. **134**, 204905 (2011).
[30] G. Tsolou, N. Stratikis, C. Baig, P. S. Stephanou, and V. G. Mavrantzas, Macromolecules **43**, 10692 (2010).
[31] S. T. Milner and J. D. Newhall, Phys. Rev. Lett. **105**, 208302 (2010).
[32] J. Qin and S. T. Milner, Soft Matter **7**, 10676 (2011).
[33] J. D. Weeks, D. Chandler, and H. C. Andersen, J. Chem. Phys. **54**, 5237 (1971).
[34] D. C. Morse and J. K. Chung, J. Chem. Phys. **130**, 224901 (2009).
[35] J. Qin and D. C. Morse, J. Chem. Phys. **130**, 224902 (2009).
[36] J. Ramírez, S. K. Sukumaran, B. Vorselaars, and A. E. Likhtman, J. Chem. Phys. **133**, 154103 (2010).
[37] J. Qin and S. T. Milner, Macromolecules **47**, 6077 (2014).
[38] W. Bisbee, J. Qin, and S. T. Milner, Macromolecules **44**, 8792 (2011).
[39] Y. Lu, L. An, S.-Q. Wang, and Z.-G. Wang, ACS Macro Lett. **3**, 569 (2014).
[40] J. Cao and A. E. Likhtman, ACS Macro Letters **4**, 1376 (2015).